Dynamic Modeling of High Bypass Ratio Turbofan Engines

J. C. Breaks*
Lockheed-California Company, Burbank, Calif.

The models described in this paper were constructed and tested as part of the wind-tunnel flutter test program for the Lockheed L-1011 Tri-Jet. This paper is presented to show the methods used to simulate the complex structure of a large turbofan engine and to present data from the calibration and test of the models which will support the conclusion that a successful simulation was accomplished. Design of the models parallels that of the full-scale Rolls-Royce RB.211 engine as closely as possible in order to permit the study of a wide range of failed and unfailed conditions. Several design compromises were necessary, however, and these and their solutions are noted. The resultant engine models proved to be very durable, undergoing over 200 hr of testing without a failure.

Introduction

THE advanced technology commercial transports now being built require engines with a large thrust capability. To achieve the thrust levels necessary, engines become large and involve rotating masses possessing gyroscopic and aerodynamic properties which could have a significant effect on the airplane wing/pylon/engine dynamic system.

In partial fulfillment of FAA requirements that new commercial transports be demonstrated free from flutter and divergence, dynamic models of the Rolls-Royce RB.211 engine were constructed and tested as part of the L-1011 Tristar development program. This paper is presented to show the methods used to simulate the complex structure of a large turbofan engine and to present data from the calibration and test of the models which will support the conclusion that a successful simulation was accomplished. These models were tested on a sting-balance mount to gather static stability and dynamic response data on the isolated engine/pylon assembly. The effect of the engine thrust and rotating mass on the wing/body system was determined with the models mounted at the wing engine stations of a similarly scaled full span L-1011 flutter model.

Design

Simulation of the entire structure of the RB.211 engine at a scale of 0.045 would have been impossible. For these models the full scale structure was consolidated and simplified as much as possible without sacrificing the ability to actually simulate the full scale engine in failed and unfailed conditions. The final models contained provisions for varying the following parameters: engine fan rotation speed, front bearing failure, engine fan shaft stiffness, engine to pylon mounts stiffness, pylon stiffness, engine fan blade angle, engine fan unbalance, core engine to fan duct connecting stiffness, and, fan duct length.

The engine models were designed to be compatible with an 0.045 scale full span L-1011 flutter model which was built lighter and less stiff than a straight-forward scaling in order to account for the effect of Mach number on the wing lift curve slope. This correction is equal to the ratio of the lift curve slope at high Mach number to the lift curve slope at the wind-tunnel Mach number and is applied to the density scale factor. Since other scale factors are dependent on the density ratio (Table 1) they are changed as well. While this correction was not necessary for the dynamic engine simulation, compatibility with the existing full span flutter model was desirable and the correction was felt to make the model test results more conservative. Reduction of model weight and stiffness by 32% resulted in a model decidedly more difficult to construct.

Engine and Subassemblies

Engine mass properties were lumped in two major subassemblies (Fig. 1); the core engine and the fan duct. The core engine contained the fan/hub, drive shaft and drive turbine described in the next section plus associated bearings and instrumentation in an aluminum shell. This assembly was mounted inside the duct on aluminum flexures which simulated the stiffness of the actual internal connecting structure. The duct was fabricated of an aluminum cylinder with fiberglass covered, balsa wood inlet and external contours and possessed scaled mass and geometric properties. Table 2 presents the results of mass and inertia measurements on an assembled engine and on these subassemblies.

That portion of the duct forward of the fan plane was removable and the resulting shortened duct permitted the simulation of either an inlet failure on the wing engine or the normal aerodynamic configuration of the center engine. Additionally, duct length was varied during the static stability testing.

Four individual flexures, oriented vertically and horizontally in groups of two, connected the core engine and duct. This orientation permitted the use of different flexure size in the two planes and allowed simulation of the differing pitch and yaw stiffnesses resulting from the failure of the engine "A" frame connecting structure. A special rig permitted calibration of the flexures in the as-installed condition. Moments were applied at the fan face

Table 1 Model scale factors

Parameter	Symbol	Value
Length	λ	0.045
Velocity (true)	V	0.1649
Density	σ	1.2365
Frequency	$f = V/\lambda$	3.6644
Dynamic pressure	$q = \sigma V^2$	0.03362
Mass (weight)	$W = \sigma\lambda^3$	1.127×10^{-4}
Unbalance	$S = \sigma\lambda^4$	5.070×10^{-6}
Moment of inertia	$I = \sigma\lambda^5$	2.281×10^{-7}
Stiffness	$EI = GJ = \sigma\lambda^4 V^2$	0.138×10^{-6}

Presented as Paper 72-376 at the AIAA/ASME/SAE 13th Structures, Structural Dynamics, and Materials Conference, San Antonio, Texas, April 10–12, 1972; submitted May 15, 1972; revision received April 2, 1973. The author wishes to thank R. F. O'Connell and V. G. Rockhold, and members of the Flight Dynamics and Wind Tunnel Departments of the Lockheed-California Co. for their aid and support during the preparation of this paper.

Index category: Aircraft Testing (Including Component Wind Tunnel Testing).

*Dynamicist.

Table 2 Mass data

Parameter		Typical Core engine	Duct	Assembled engine
Weight ~ grams				
	actual	412	235	668
	target	415	267	696
C.G. location on ℄ ~ in.				
	actual station	6.65	4.92	5.99
	target station	6.83	4.81	6.00
Inertia ~ gram-in.^{2}				
I_x (roll)	actual	247	1075	1410
	target	225	1061	1346
I_y (pitch)	actual	4335	1377	4070
	target	4064	1196	3720
I_z (yaw)	actual	4305	1262	3910
	target	4016	1144	3625

and relative rotation between the core engine and duct was measured. Presentation of results is in Table 3.

Rotating Mass

Rotating mass in the RB.211 is limited to the core engine and consists of three compressor-turbine assemblies mounted on separate co-axial shafts and operating at different rotational speeds. The 33-blade bypass fan and its drive are, of necessity, mounted on the longest shaft and include the largest portion of the rotating mass. Model size prevented simulating all of the rotating parts at their speeds and necessitated the selective compression and simplification of this structure. The final model configuration consisted of a single-stage air turbine driving a 12-bladed fan and simulated the full scale engine rotational inertia and total moments of momentum (the fan cruise RPM was 14,200 model; 3881 full-scale). Assembled engines produced scale thrust within 10% and so simulated actual mass flow through the engine.

The 33 blades on the full-scale fan were reduced to 12 on the model with a concurrent increase in blade chord length to keep a simulated total blade area. By reducing the number of blades to 12 it was possible to simplify the hub fabrication process and still provide an adequate simulation of the blade aerodynamic forces necessary for a realistic gyroscopics investigation. Individual aluminum blades were provided with a cylindrical stub base and were clamped into the hub. Blade incidence angle could be varied from approximately 10° to 60° at the tip by rotating the blade base within the hub and then reclamping in the hub.

Complete loss of one full-scale fan blade could be simulated by installing a shortened fan blade in the model. This blade was installed in place of a regular blade and provided model unbalance of 0.76 gm-in.

An aluminum shaft, supported by ball bearings at three locations, connected the hub assembly to the air turbine

Table 3 Flexure stiffness data

Core duct flexure	Due to . . . . ing moment Pitch	Yaw	Roll
Unfailed			
actual	5.7	5.7	6.16
target	5.87	5.81	6.03
Failed "A" frames			
actual	9.45	7.57	35.44
target	8.35	7.86	36.3

all × 10^{-4} rad./in.-lb.

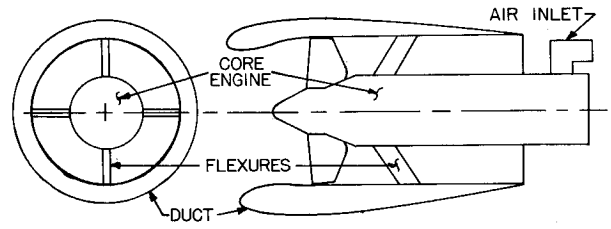

Fig. 1 Engine subassemblies.

(Fig. 2). By removing the forward-most shaft-support bearing the effects of an engine front bearing failure could be simulated. Drive shafts of different diameters could then be installed to provide varying amounts of mounting stiffness for the fan/hub assembly. Unit forces and moments applied at the fan plane on a shaft of nominal stiffness produced the fan rotations and deflections noted in Table 4. For these calibrations the shaft was mounted on bearings in a rig designed to reproduce the support characteristics of the shaft as installed in the engine. Other available shafts 1/3, 1/2 and 2/3 nominal stiffness, exhibited similar target matching.

The rotational moment of inertia of the fan, shaft and turbine assembly was brought up to target value with a mallory metal ring attached to the magnesium air motor turbine. Measurements of this roll moment of inertia yielded 89.96 gm-in.^{2} The computed total moment of momentum was, also, within 3% of the target. Other mass properties of this assembly were not matched but are included in the data for the core engine assembly.

Dynamic balancing of the rotating assemblies was performed at the Lockheed Rye Canyon Research Center. Final unbalance of these assemblies did not exceed 0.2 gm-in.

Engine Mountings

Two types of pylon mounting systems were used to carry the engine assembly. A one point, rigid attachment was provided for tests involving pylon stiffness variations. This design included the pylon and engine mount stiffness in a single cruciform beam with the pylon attached to the fan duct at one point, see Fig. 3. Fabrication of ten of this type pylon permitted vertical and lateral stiffness variations over a matrix of values from 0.3 to 1.2 times standard. Primary interest was in first vertical and lateral bending frequencies of the engine/pylon assembly and this family of pylons produced variations of these frequencies in the order of a factor of 2.

A second system, Fig. 4, provided a more precise representation of the actual engine mounting system by separating the total mounting stiffness into pylon and forward and aft engine mount components. The pylon for this complex system contained two separate beam sections and simulated full-scale pylon stiffness between the two engine mounts and between the aft mount and the wing attachment. Individual engine mounts were pinned link structures resembling the full-scale mounts.

The forward mount, shown in Fig. 5, resisted only translational forces and was relatively flexible to mo-

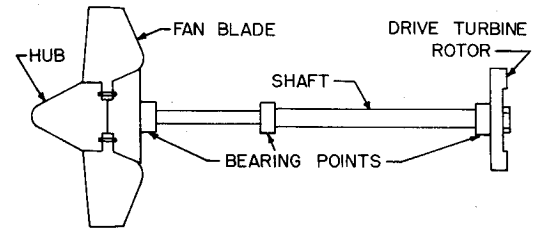

Fig. 2 Rotating parts.

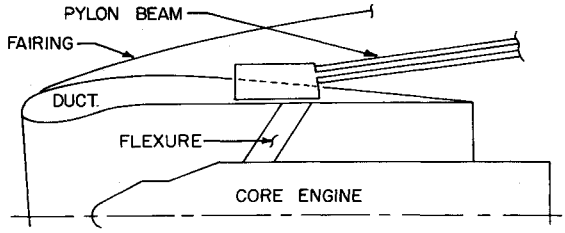

Fig. 3 Simple pylon mount.

ments. A vertical slot at one center leg connection allowed side and normal forces to be resisted by the outer legs while fore and aft movement in the outer leg pins permitted axial force resistance from the center leg only.

The aft mount, Fig. 6, resisted normal and side forces and rolling moment and was relatively weak to other forces and moments. Fashioning mount structure in the shape of an inverted "Y" resulted in primary resistance to normal force and rolling moment by the upper horizontal beam and to side force by the legs. Pivots at the leg ends combined with thinness of the legs, produced relative weakness to other load components.

Mounts were tested individually for stiffness levels. Light beams reflected from mirrors placed on the mount were monitored during loading to assure that movements out of the measurement plane were minimized. Even with these precautions the magnitude of the deflections encountered was small and measurement errors were relatively large (10 to 40% of the measurement). Stiffness of the individual mounts was secondary to the ability of these mounts to simulate the gross changes resulting from the failure of a supporting link. It was desirable, of course, to have the assembled complex pylon-mounts-engine system exhibit modal frequencies similar to those of the corresponding simple pylon system. Since these frequencies were at the proper levels, the stiffness of the mounts was considered acceptable.

Complex pylon calibration results are presented in Table 5. The data are referenced to the engine mount/pylon interfacing surface and show good agreement with targets extending even to the off diagonal terms.

Calibration Methods

Calibration data presented in the previous sections of this paper were obtained with the standard projected grid and mirror system for rotational deflections and a machinist's dial indicator for linear displacement. Moment of inertia was determined by properly orienting the part or assembly on a bifilar pendulum, timing the period of oscillation and computing results. The pendulum constant was computed and then checked empirically with a body of easily calculable inertia.

Engine Instrumentation and Control

Instrumentation was uncomplicated and consisted of vertically and laterally oriented strain gage bridges on the pylon beam, devices to measure engine speed and fan/hub

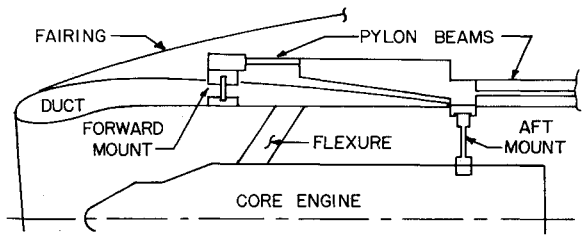

Fig. 4 Complex pylon mount.

Table 4 Nominal engine shaft stiffness data

	Target		Actual	
	Side force $Y \sim$ lb	Yaw mom $N \sim$ in.-lb	Y	N
y deflection $\sim$ in.	0.02682	0.01519	0.0271	0.0149
ψ rotation $\sim$ rad.	0.01519	0.00922	0.0139	0.0087

activity and, for unbalanced fan conditions, accelerometers on the core engine. Fan rotational speed was determined by a magnetic proximity pickup sensing 12 steel pins in the air turbine rotor. An electrical signal was transmitted to a digital counter which displayed fan speed in RPM. Another proximity pickup was mounted in the shaft support structure of the core engine and sensed the nearness of a steel ring on the rear face of the fan hub. Wobbling of the hub was then translated into varying electrical signals which could be recorded on FM tape or displayed on an oscilloscope.

At all times during the operation of these models TV video tape systems monitored and recorded model condition and activity. High speed motion picture cameras were also available and could be activated remotely to document selected instances of model activity.

The engine control system depicted in Fig. 7 provided filtered air at a regulated pressure to the engines and possessed several model protection features. Automatic systems monitored engine RPM as well as the voltage level of the tachometer signal and if either parameter exceeded a preset level, the gate valve on the air supply would be closed. For this application, an over voltage could be produced by either overspeed or too rapid acceleration of the engine. Under normal conditions engine RPM was monitored on a display and the regulator valve was controlled manually.

The method of powering the engine through air supply lines leading from the model proved to have little effect on the data obtained. Before testing began, the potential for interaction was checked by blocking off the air line at the model and then pressurizing the line. With the model engine/pylon assembly mounted on the balance, pressure in the line produced a very slight shift in axial force and had no effect on other components. After installing the model assembly for dynamic response testing, vibration modes were surveyed for frequency and damping rate with no air line installed and with an air line pressurized and

Table 5 Complex pylon deflection matrix

		TARGET						
		UNIT LOAD AT						
		FRONT MOUNT			REAR MOUNT			
		X ~LB	Y ~LB	Z ~LB	Y ~LB	Z ~LB	ROLL MOM. ~IN-LB
ACTUAL		61	5	-159	-6	-44	-8
			6450	181	1712	78	-694
DEFLECTION AT FRONT MOUNT	X~IN. 0			3589	148	667	160
	Y~IN. -	6075			866	68	-120
	Z~IN. -200	120	3550			292	73
DEFLECTION AT REAR MOUNT	Y~IN. -	2250	30	940			649
	Z~IN. 0	0	700	30	325		
	Ø~RAD. -	-375	-	-40	-	582	

ALL VALUES X 10^{-5}

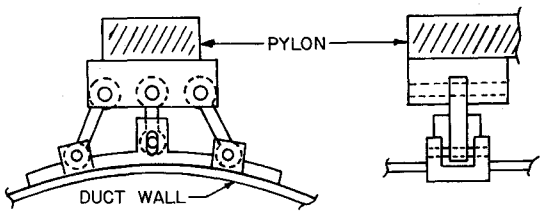

Fig. 5 Forward mount geometry.

unpressurized. With no air line the modal frequencies were sharp and modes of primary interest had damping rates of $g < 1\%$. Adding a pressurized air line changed modal frequencies only slightly but did increase damping levels to the 2% to 3% range.

Testing

Testing of the models was conducted in the Lockheed-California Company 8- × 12-ft Low Speed Wind Tunnel at Burbank, Calif., and can be separated into three phases. In the first phase of testing a model engine/pylon assembly was mounted to a sting-supported six-component strain gage balance. Initial runs were made with no flow in the wind-tunnel. Force data were taken at various model power settings and from these data Fig. 8 was generated. Aerodynamic force data were obtained at a wind-tunnel dynamic pressure, q, of 40 PSF with the models powered and windmilling. From these data static aerodynamic derivatives were determined for the complete engine, the engine with short duct and the core engine alone. Two different balance systems were used; the second to improve resolution of forces.

An engine/pylon assembly was attached to the same sting mount for the investigation of isolated engine dynamic response conducted in phase two. Variables of interest were pylon stiffness, duct length, engine shaft stiffness, fan unbalance and front bearing failure. Dynamic response runs were typically conducted by setting engine RPM at 14,200 (cruise simulation) and then slowly increasing tunnel speed until an instability occurred or until a maximum dynamic pressure was reached. This maximum q was determined by the necessity of clearing to 1.2 times the design velocity ($\approx$40 PSF) for unfailed conditions or the design velocity ($\approx$30 PSF) for single failure conditions. If the maximum q was reached without instability the engine RPM was reduced to windmilling speed while tunnel q was maintained.

During a run, damping of the model motions was determined by manually exciting the model and noting the decay rate of the resultant oscillations. Excitation was accomplished through fine wires attached to the model and led outside the tunnel. Either lateral or vertical movement could be induced by using one or the other of the two wires installed. These wires also proved useful for stopping potentially damaging oscillations.

Upon completion of the sting mount portion of the test, the 0.045-scale full span flutter model was installed in the tunnel. This model was mounted on a two-wire support system, with four snubber cables, and within these limits was free flying. Dynamically-scaled engines were mounted on each wing, with the air supply lines and instrumentation cables routed down the lower snubber cables. Wires for manual excitation of the engine were installed and runs were conducted as in phase two. Airplane configuration changes were limited to wing fuel quantity but engine variables included front bearing failure, duct length, internal core engine to fan duct stiffness, engine shaft stiffness, fan unbalance and engine mount failures, i.e., removal of various links on individual engine mounts.

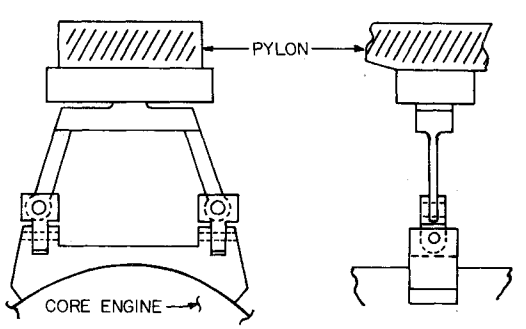

Fig. 6 Aft mount geometry.

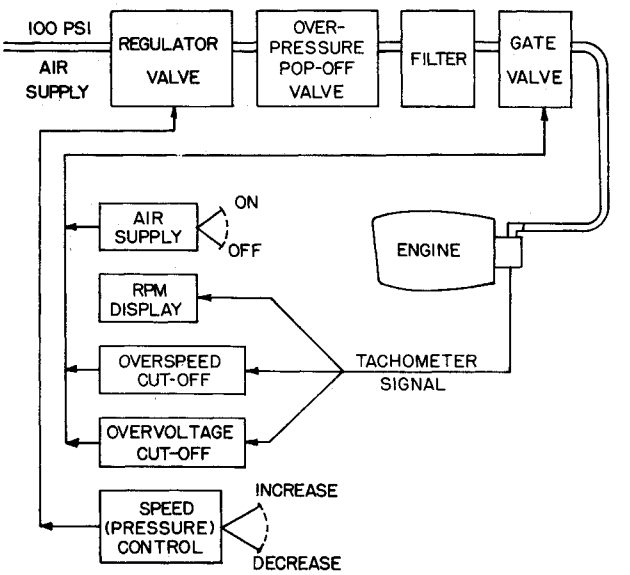

Fig. 7 Engine control system.

Analysis

Model calibrations and test data were checked by using standard vibration and flutter analyses, with target data and actual model data as inputs. The analytical model had 16 final degrees of freedom derived from an initial 30 engine compliances plus 6 pylon compliances (12 for a complex pylon). Aerodynamic coefficients were deter-

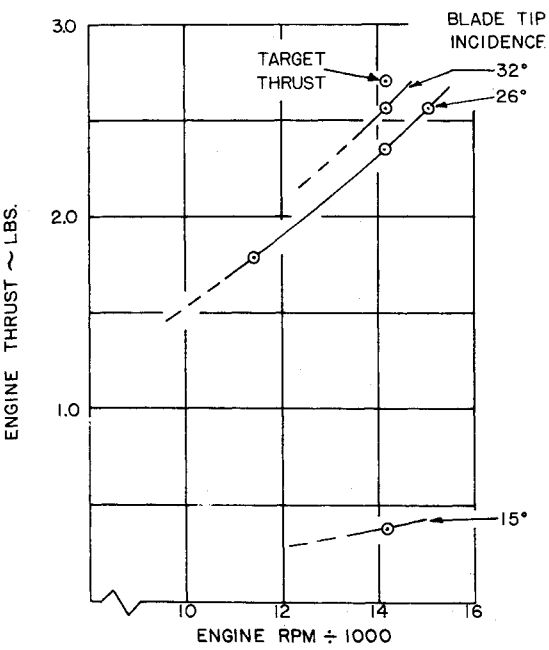

Fig. 8 Engine performance.

Table 6 Frequency survey cantilevered simple pylons

Mode	Standard stiffness pylon		Reduced stiffness (0.8 std) pylon	
	Analysis	Test	Analysis	Test
Lateral bending	11.27 Hz.	11.4 Hz.	9.95 Hz.	9.8 Hz.
Vertical bending	12.97	13.2	11.36	11.2
Roll/yaw	20.94	23.0	19.03	19.8
Engine pitch	32.70	30.8	31.42	28.7
Yaw/roll	58.77	58.9	55.69	54.4

mined during the force phase of model testing. However, because of data scatter and the difficulty of separating fan and duct coefficients, it was decided to use coefficients obtained with a Lockheed-developed nonviscous potential flow theory which included compressibility effects. Comparison of analytical results obtained with target data input and those obtained with model data input indicated no significant effect due to model deviations from the targets.

Results

A detailed examination of data from a test program of this size is beyond the scope of this paper. However, a cursory look at typical results is in order. Throughout the testing the primary goal was to simulate and test realistic engine configurations and to demonstrate freedom from flutter and divergence to the limits required by the FAA. Additionally, data for comparison with analysis were to be obtained by introducing unrealistically severe model failures in order to induce whirl flutter.

After calibration for deflection and rotation, described in previous sections, pylon/engine assemblies were cantilevered and surveyed to determine the fundamental vibration modes and their frequencies. Results of surveys conducted on two simple pylons and vibration analyses made using calibration results as input are presented in Table 6. These pylons are from the group of ten simple pylons used for the study of pylon stiffness effects and simulate standard stiffness for an unfailed pylon and 80% standard lateral and vertical stiffness for a failed pylon. Other pylons in the group exhibited similar frequency matching. An additional frequency survey was made for each configuration with the model installed on the wind-tunnel support system. Results of a typical survey, conducted on an isolated standard pylon and engine assembly, plus the vibration analysis of the assembly with proper model-support flexibility are presented in Table 7.

Mode shapes mentioned in Tables 6 and 7 are typical of an assembly with the engine mass mounted at the end of a pylon beam. Lateral and vertical bending are merely pylon first bending modes and engine pitch is a pylon second bending mode which results in more pitching motion of the engine. The two yaw/roll modes result from the engine center-of-gravity being below the pylon axis. Both of these modes involve large amounts of roll and yaw movement but the lower mode has relatively more roll and the higher has relatively more yaw.

Preliminary analyses had shown that whirl flutter type instabilities could be expected on configurations with the front engine bearing removed and engine shafts of reduced stiffness. Removal of the front engine bearing produced a fan pitch mode characterized as an engine shaft 1st bending and resulting in fan assembly translation and rotation. Prior to runs involving this configuration surveys were made to determine the frequency and damping of this fan mode. These surveys and analysis of the system, produced the following: standard stiffness shaft, 40.9 Hz from test (40.72 Hz from analysis); 2/3 standard stiffness shaft, 38.0 Hz (38.2 Hz); 1/3 standard stiffness shaft, 29.2 Hz (28.49 Hz). Structural damping for this mode was from $g = 0.5\%$ to $g = 0.75\%$.

Table 7 Frequency survey standard pylon on tunnel support system

Mode	Analysis	Standard engine/pylon assembly in tunnel
Lateral bending	9.59 Hz.	10.0 Hz.
Vertical bending	10.80	11.0
Roll/yaw	18.39	19.4
Engine pitch	30.58	30.3
Yaw/roll	51.06	51.4

Whirl flutter points were obtained experimentally in several instances. In all of these cases the fan whirl was localized because the simulated severe failures, which were necessary to induce the oscillation, decoupled the fan from the rest of the engine. No instability could be induced on any configuration representative of the full-scale RB.211 engine in either failed or unfailed condition.

The most thoroughly documented instance of whirl flutter occurred on a configuration with an engine shaft stiffness of 1/3 standard and a failed forward bearing. Analysis of this configuration indicated a fan backward whirl instability would occur at a dynamic pressure of 6.0 PSF and a frequency of 6.8 Hz. The actual model instability was backward whirl and occurred at a dynamic pressure of 4.9 PSF and a frequency of 6.0-6.5 Hz. Additional runs on the model showed that minor changes in the engine angle-of-attack, fan blade incidence angle or engine power setting had major effects on the whirl flutter point, in all instances delaying or eliminating the onset of instability.

Conclusions

Purposes of testing were threefold: first to comply with FAA requirements in the certification of the L-1011 airplane; second, to obtain static aerodynamic derivative data on various nacelle configurations to check and refine methods to determine these derivatives for analysis; third, to obtain whirl flutter by introducing multiple model failures for the purpose of comparison with analysis. The models were designed, fabricated and calibrated at the Lockheed Fluid Dynamics Laboratory. Results of these calibrations, plus analyses and testing, permit the following conclusions:

Accurate structural and stiffness simulations of large turbofan engines are possible with small models. These models are durable and are capable of simulating a large range of failed and unfailed conditions, thrust levels, blade angles and RPM levels. Only one engine had the capability of being mounted on both simple and complex mounting systems. This primary engine was used for most of the testing, and although no instabilities were encountered during any tests representative of either the intact or failed RB.211 engine, four cases of gyroscopic instability were induced by removing the fan shaft forward bearing and installing fan shafts of severely reduced stiffness. No primary engine whirl flutter could be induced on any configuration representative of the airplane. The only model damage incurred during testing was an engine shaft bent at the first encounter of a gyroscopic instability.

Aerodynamic derivatives of interest ($C_{\gamma\alpha}$ and C_Z/C_{Z_Ψ}) could not be resolved by the first balance system used and were marginally within the limits of resolution of the second balance. Additional studies of derivative determination are being conducted as time and funds become available.

Engine dynamic instabilities were obtained and were predicted by a whirl flutter analysis.